An Improved Droop Control Method for Multi-Terminal VSC-HVDC Converter Stations

Hao Wang [1,2], Yue Wang [1], Guozhao Duan [1], Weihao Hu [2,*], Wenti Wang [1] and Zhe Chen [2]

[1] Power Electronics & Renewable Energy Research Center, Xi'an Jiaotong University, No. 28, Xianning West Road, Xi'an 710049, China; wan@et.aau.dk (H.W.); yuewang@mail.xjtu.edu.cn (Y.W.); guozhao_duan@163.com (G.D.); wentiwang@stu.xjtu.edu.cn (W.W.)

[2] Department of Energy Technology, Aalborg University, Pontoppidanstraede 101, Aalborg DK-9220, Denmark; zch@et.aau.dk

[*] Correspondence: whu@et.aau.dk; Tel.: +45-2137-0382

Abstract: Multi-terminal high voltage direct current transmission based on voltage source converter (VSC-HVDC) grids can connect non-synchronous alternating current (AC) grids to a hybrid alternating current and direct current (AC/DC) power system, which is one of the key technologies in the construction of smart grids. However, it is still a problem to control the converter to achieve the function of each AC system sharing the reserve capacity of the entire network. This paper proposes an improved control strategy based on the slope control of the DC voltage and AC frequency (*V–f* slope control), in which the virtual inertia is introduced. This method can ensure that each AC sub-system shares the primary frequency control function. Additionally, with the new control method, it is easy to apply the secondary frequency control method of traditional AC systems to AC/DC hybrid systems to achieve the steady control of the DC voltage and AC frequency of the whole system. Most importantly, the new control method is better than the traditional control method in terms of dynamic performance. In this paper, a new control method is proposed, and the simulation model has been established in Matlab/Simulink to verify the effectiveness of the proposed control method.

1. Introduction

In recent years, wind, solar, and other new energy technologies have developed rapidly. However, they have the characteristics of intermittence and randomness, which makes it more and more limiting for the traditional power grid to absorb ultra-large-scale renewable energies. The flexible multi-terminal DC grid technology is one of the effective techniques to solve this problem [1–7].

The traditional control strategy of converter stations focuses on the transmission power. The converter acts as a specified power supplier in the inverter side, or a load in the rectifier side. Thus, it plays a negative role in regulating the power of the entire grid [8–11]. As is well known, the purpose of traditional small-scale power grids interconnecting to larger grids is to enable each small grid to share the moment of inertia and frequency regulation function. Thus, they can support or act as a standby for each other to make the whole system more stable. If the converter stations are controlled as specified power suppliers or loads, it will greatly weaken the advantages of the interconnected system [12–14]. The proposed control strategy will solve this problem.

In order to ensure the steady operation of the multi-terminal high voltage direct current transmission based on voltage source converter (VSC-HVDC) grid, the basic control requirements are to maintain the stability of the DC voltage and to balance the DC power [15–19]. In order to keep the DC voltage stable and the system power balanced, both the voltage control and power control are

commonly used [20,21]. At present, there are three main types of voltage control strategy: the voltage margin control, the voltage droop control, and the voltage droop control with a voltage margin [22]. These three control modes can realize the coordinated control of DC voltage and power, but they are lacking in a real-time interaction for the AC networks, and cannot provide a primary frequency control function for each sub-AC grid. Thus, scholars have put forward a method that combines the DC voltage power droop with the AC frequency power droop [1,23–25]. It can sustain DC voltage and provide the primary frequency control function to a sub-AC grid [16–18]. However, this control method is lacking in a dynamic flow balance method. During a load disturbance, this control method will lead to more transient power fluctuations [26].

This article proposes an improved droop control method. With every converter station using this control method in multi-terminal VSC-HVDC system, each AC system can share the primary frequency regulation service. All the generators can share their inertia in the hybrid AC/DC power system. The real-time interaction of each AC system is enhanced. Additionally, it is easy to apply the secondary frequency control method of traditional AC systems to the AC/DC hybrid system.

This paper proposes an improved control strategy based on the slope control of the DC voltage and AC frequency (*V–f* slope control), in which the virtual inertia is introduced. This paper is arranged as follows: In Section 2, the applied models of the whole hybrid AC/DC system are presented. Based on the model, in Section 3, the control strategy and the coordination method are proposed. In Section 4, the crucial parameters of the control strategy are discussed. In Section 5, the validity of the proposed control method is proved by simulation in Matlab/Simulink. Finally, the conclusion and the future work are presented in Section 6.

2. System and Model Description

2.1. DC Grid Description

The research object of this paper adopts a bipolar-operation, three-terminal HVDC system with a star topology. The bipolar-operation, three-terminal HVDC system of this paper is a hypothetical power system. The DC-side uses a unified rated voltage of $\pm$ 200 kV. DC lines adopt lumped parameters. The line capacitance effect is focused on the DC-side of the converter and the line inductance is ignored. The structure of the power grid is shown in Figure 1.
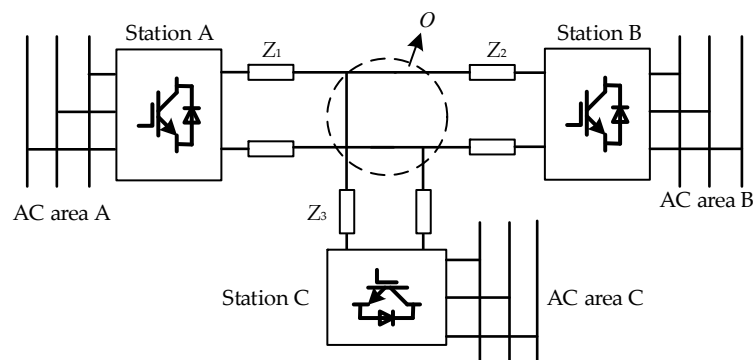

Figure 1. Structure of the multi-terminal DC grid.

In Figure 1, areas A, B and C represent three asynchronous AC power grids. Point O is a node of the DC power grid. The multi-terminal DC power grid adopts overhead lines. These lines choose aluminum cable steel reinforced (ACSR)-720/50 with R = 0.04 (Ω/km), and adopt a four-splitting lead. The distances of OA, OB and OC are 100 km, 80 km and 40 km, respectively. The resistances of each line are:

$$R_{AO} = 0.04/4 \times 100 \times 2 = 2\Omega$$
$$R_{BO} = 0.04/4 \times 80 \times 2 = 1.6\Omega \tag{1}$$
$$R_{CO} = 0.04/4 \times 40 \times 2 = 0.8\Omega$$

2.2. AC Grid Description

In Figure 1, the three AC systems A, B and C are asynchronous; each AC system is represented by an equivalent source and load. The synchronous generator model represents the power source, and the equivalent model of each AC system is shown in Figure 2.

The terminal voltage of the synchronous generator is 10 kV and it is connected to the 110 kV lines through a 10/110 kV transformer. The equivalent concentrated load and the line impedance are connected to the 110 kV line. The parameters of the AC grid are shown in Tables 1 and 2.
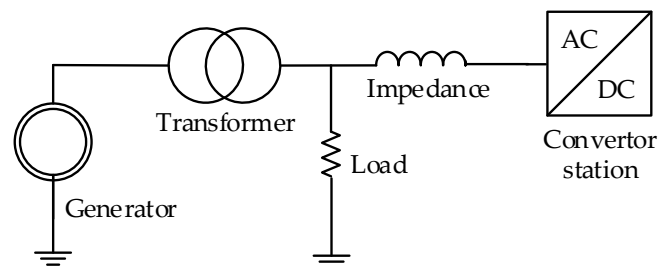

Figure 2. Control strategy diagram.

Table 1. Parameters of AC generators.

Parameters/AC Area	A	B	C
Rated power (MW)	600	400	100
Initial power (MW)	488.70	246.16	81.45
Droop coefficient (Hz/MW)	0.0042	0.0168	0.025
Inertia constant (S)	6.5	6.5	6.5

Table 2. Parameters of AC line and load.

Parameters/AC Area	A	B	C
Initial load (MW)	380	180	240
Line impedance (Ω)	4 + j12.5	4 + j12.5	4 + j12.5
Rated power of transformer (MVA)	600	400	100

In addition, 2% of the power loss is considered as output power, and it is distributed by the generators of the three areas according to per unit of their rate capacities.

2.3. Converter Station Description

In fact, typical VSC-HVDC converter stations always adopt modular multi-level topologies. The main research point of this paper is the method for the coordinated control of AC/DC power, so the control problem of the converter component level is ignored. To simplify the problem, it uses three-phase, two-level, triple-arm bridges with IGBT power semiconductors to replace the actual modular multi-level topology model.

3. Proposed Control Method

The new control method is based on the speed droop characteristics of traditional AC power grids and the voltage droop control of traditional HVDC converter stations; thus, it inherits the characteristics of the two traditional control methods.

For VSC-HVDC transmission systems, it is assumed that the converter station V_2 is connected to the stable DC grid V_1 through line impedance, as shown in Figure 3.
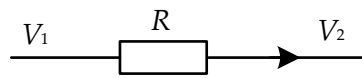
Figure 3. Equivalent connection of the DC grid and converter station.

The transmission power from the DC grid to the converter can be expressed by Equation (2):

$$P_2 = \frac{\Delta V}{R}(V_1 - \Delta V) \tag{2}$$

where P_2 is the transmission power of the converter station, V_1 is the voltage of the DC grid, and V_2 is the DC-side voltage of the converter station.

In Equation (2), if ΔV is much less than V_1, it can be ignored; then Equation (2) can be turned into Equation (3):

$$P_2 \approx \frac{\Delta V}{R}V_1 = \frac{V_1^2}{R} - \frac{V_1}{R}V_2 \tag{3}$$

From Equation (3), it can be illustrated that the power transferred from the DC grid to the AC area is inversely proportional to the voltage of the DC terminal. If $V_2 < V_1$, the converter acts as an inverter; otherwise, it acts as a rectifier. The characteristics are shown in Figure 4.
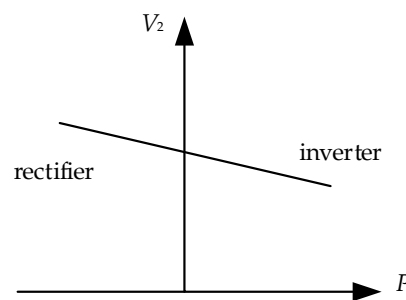
Figure 4. Operation characteristics of the transmission power and the DC-side voltage.

If the inverter acts as a power supplier in the AC side. It should be operated by the frequency and active power droop control to provide a primary frequency control function for the AC system. From the view of the rectifier side, it acts as a load of the AC-side. The control characteristic is that the frequency and active power are in a positive correlation. Therefore, the ideal control characteristic of the active power and frequency is shown in Figure 5.

As shown in Figures 4 and 5, if the converter station operates in the inverter state, when the frequency of the AC system decreases, the AC side hopes to obtain more active power to support its frequency; thus, it requires the terminal voltage of the DC-side to be decreased to satisfy a more active power transmission. When the frequency of the AC system increases, the AC-side hopes to obtain less active power and the terminal voltage of the DC-side should be increased. This requires the AC system frequency and DC voltage control to positively correlate, as Figure 6 shows.

If the converter station operates in the rectifier state, the control principle is the same as for the inverter state.
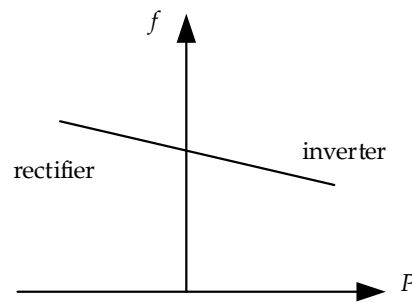
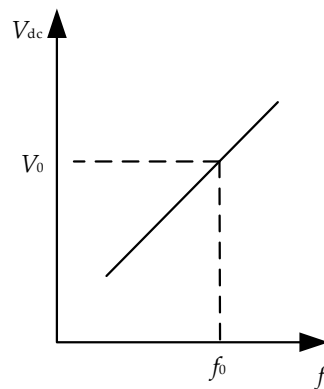**Figure 5.** Control characteristics of the converter station.

Figure 6. The positive relationship between the DC voltage and AC frequency.

Based on the analysis above, this paper proposes a control method. It puts the converter DC voltage and AC frequency in a positive relationship, as shown in Figure 6. In addition, to make the converter automatically sense frequency fluctuations of the AC system and supply energy to AC grids, the converter should make the AC frequency as feedback in the outer control loop. The virtual inertia is introduced in the control strategy, which makes the converter achieve dynamic power sharing, as for the traditional synchronous generator when a load disturbance occurs in the AC system [26,27]. Additionally, to ensure that the converter has the ability to support DC voltage, the converter should also make DC voltage a feedback in the outer control loop. The control loop is shown in Figure 7.
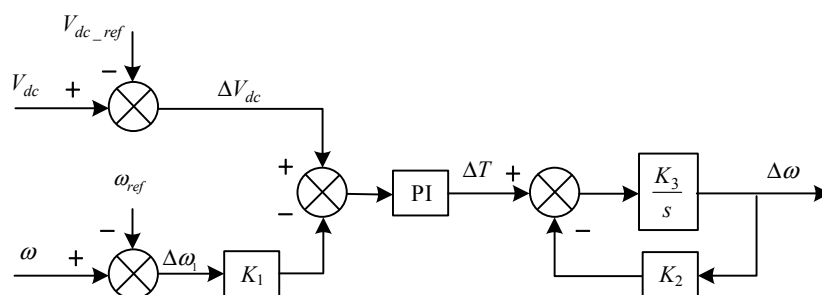

Figure 7. The control loop of the DC voltage and AC frequency.

In Figure 7, ω is the sampled AC frequency; ω_{ref} is the reference AC frequency, which equals 100π rad/s; $V_{\text{dc\_ref}}$ is the reference DC voltage of the converter station; and K_1 is the slope coefficient of the AC frequency and DC voltage. When there is a need for AC systems to share the primary frequency regulation service, K_1 can regulate the dynamic power that each AC system should undertake. The transfer functions, Equations (4) and (5), can be obtained from Figure 7:

$$\Delta T = (\Delta V_{dc} - K_1 \cdot \Delta\omega) \cdot (\frac{K_i}{S} + K_p) \tag{4}$$

$$\frac{\Delta\omega}{\Delta T} = \frac{1}{S/K_3 + K_2} \tag{5}$$

where K_p and K_i are the coefficients of the proportional-integral (PI) controller, ΔT is the intermediate variable, and K_2 and K_3 are the virtual inertia coefficients. These should be designed carefully to provide virtual inertia to AC grids.

4. Parameter Designs

The parameters of the new control method for the VSC-HVDC converter station are K_1, K_2, K_3, K_p and K_i. A suitable K_1 can sustain the AC frequency and DC voltage both at the scheduled level when the load increases suddenly in one AC system (as for the simulation presented in Section 5.1). The reasonable design of parameters K_2, K_3, K_p and K_i can smooth the frequency fluctuation of the AC system. The design principle should be based on the premise of satisfying the dynamic power sharing, and then making full use of the inertia of all generators in the entire system.

4.1. The Design of Slope Coefficient K_1

The DC voltage and AC frequency slope coefficient K_1 is a key parameter in the new control method. It has a similar design principle to the typical speed-droop characteristics of traditional power plants. With respect to the typical speed-droop characteristics of traditional power plants, it requires a load fluctuation ΔP within the range of $\pm 5\%$; the whole range of primary frequency control is released when the frequency error is about ± 200 mHz. Therefore, the speed-droop coefficient K is the ratio of the maximum relative power fluctuation and the maximum frequency relative deviation [23]. The speed-droop coefficient is calculated by Equation (6):

$$K = \frac{\Delta P/P_n}{\Delta f/f_n} \tag{6}$$

where K is the speed-droop coefficient, P_n is the active power of the AC system, and f_n is the rated frequency.

The method of designing the *V–f* control slope coefficient K_1 is proposed—refer to the typical speed-droop coefficient design of K. K_1 can be determined by the ratio of the maximum DC voltage relative deviation and the maximum frequency relative deviation. It can make the most of the permissible fluctuations of the DC voltage and AC frequency. It can be expressed by Equation (7). In this way, the slope coefficient of every converter station is equal. In fact, with respect to a multi-terminal VSC-HVDC system, the line impendence is very small, which results in a small deviation of the DC voltage among different converter stations.

$$K_1 = \frac{\Delta V/V_n}{\Delta\omega/\omega_n} \tag{7}$$

It is assumed that the maximum DC voltage relative deviation is 10%. The frequency relative deviation is kept the same as for the traditional AC system (± 200 mHz), and the base frequency is 50 Hz. The slope coefficient K_1 can be calculated to be 25 from Equation (7).

4.2. The Design of Inertial Coefficients K_2 and K_3

A reasonable design for the inertial coefficients can make the VSC-HVDC converters provide a virtual inertia to AC grids that is similar to that of the traditional synchronous generators. The virtual inertia plays an important role in damping the high frequency fluctuation of power, and smoothing the frequency variation in transient processes. Several studies have investigated the virtual inertia of virtual synchronous generators (VSGs). These generally made the virtual inertia coefficient equal

to the moment of inertia of the synchronous generator, realizing the power sharing in the dynamic processes [26,27]. Therefore, the time constant of the converter's frequency loop should equal the inertia time constant of the generator to achieve similar characteristics to the synchronous generator. In Figure 7, the relationship between $\Delta\omega$ and ΔT is expressed as Equation (5), while the swing equation of the generator can be expressed as Equation (8) [28]:

$$\frac{\Delta\omega}{\Delta T} = \frac{1}{D + J \cdot S} \tag{8}$$

where $\Delta\omega$ is the frequency deviation, ΔT is the deference of the turbine torque and the electromagnetic torque, D is damping torque coefficient, and J is the moment of inertia of the generator.

In fact, Equations (5) and (8) have a similar form. In Equation (5), the time constant of the frequency loop is $K_2 \cdot K_3$, making it equal to the inertia time constant of the generator. In this situation, the converters can provide virtual inertia to AC grids. A reasonable number for the inertia time constant is 5.2 [28]. Thus, Equation (9) can be obtained:

$$K_2 \cdot K_3 = 5.2 \tag{9}$$

This paper assumes that $K_2 = 1$; thus $K_3 = 5.2$, according to Equation (9).

4.3. The Design of the Reference DC Voltage of Each Converter

When setting the reference DC voltage of the converter station, the transfer power should be considered. Assuming point O (Figure 1) is the center, the voltage at point O is kept at 400 kV. In the initial state, the power of the generator in area A is 488.7 MW, and the load is 380 MW. Thus, area A needs to transfer 108.7 MW to the DC grid. Because point O is 400 kV, and the resistance from point O to station A is 2 Ω, the reference DC voltage of station A can be found from Equation (10):

$$\frac{108.7}{400} \times 2 + 400 = 400.54 \tag{10}$$

Using the same method, the voltages of station B and C can be found; they are 400.26 kV and 399.68 kV. The parameters of the converter station are shown in Table 3.

Table 3. Parameters of the converter station.

Parameters/AC Area	A	B	C
K_1	25	25	25
K_2	1	1	1
K_3	5.2	5.2	5.2
K_P	1	1	1
K_i	100	100	100
$V_{\text{dc\_ref}}$ (kV)	400.54	400.26	399.68

Additionally, with respect to the AC voltage amplitude control, this study uses reactive power and voltage droop control [28]. The method of designing the droop coefficient is similar to that for the speed-droop coefficient, which was described in Section 4.1. The reactive power and voltage droop coefficient can be described mathematically by Equation (11) [28]:

$$K_Q = \frac{\Delta Q / S_n}{\Delta V / V_n} \tag{11}$$

where K_Q is the reactive power and voltage droop coefficient, S_n is the rating of the AC grid, and V_n is the rated AC voltage.

5. Simulation Study

To evaluate the proposed converter control strategy, an AC/DC hybrid parallel system model was built in Matlab/Simulink. For a special explanation, this control method was used for all converter stations in multi-terminal VSC-HVDCs. Two important functions were achieved by applying the new method. The first function was that it could realize asynchronous AC systems sharing their primary frequency control functions. The second function was that it was easy to apply the secondary frequency control method of traditional AC systems to the AC/DC hybrid system.

To evaluate the advantages of the proposed method, it was compared with the traditional *V–f* control method. The traditional *V–f* control method is proposed by reference [25].

5.1. Load Disturbances

At 10 s, a load increase of 45 MW in area C was simulated. Before *t* = 10 s, area A and area B transmitted 100 MW and 60 MW of active power to area C through the DC grid, respectively. At *t* = 10 s, the load in area C increased 45 MW suddenly; the response waves of the frequency of each AC area, the DC-side voltage, and the transmission power of each converter are shown in Figure 8. The response of the traditional control method [25] is shown in Figure 9.
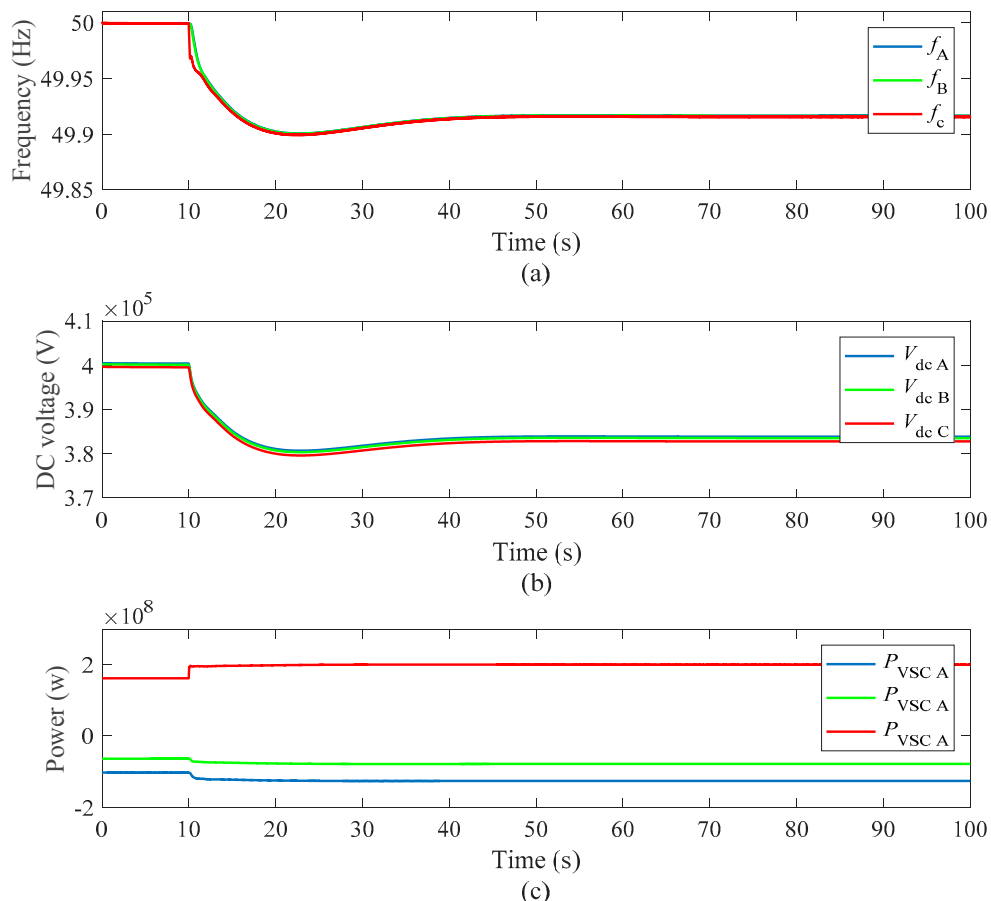

Figure 8. The waveforms of disturbances occurring in area C: (**a**) AC frequency of each sub-AC system; (**b**) DC-side voltage of each converter station; and (**c**) transmission power of each converter station.

In Figure 8, from the frequency waveform, when the load disturbance occurred in area C at 10 s, the frequencies of areas A, B and C decreased. With the frequencies decreasing, the generators of the three areas increased their active power outputs due to the effect of the frequency droop control of the generators. From the power waveform, when a load step occurred in area C, areas A and B transferred

more active power to area C automatically, to balance the power of the entire system. Thus, areas A and B shared their primary frequency control function with area C. Because the three converter stations used the same control method, we can suppose that if the load increase occurred in area A or B, it is reasonable to consider that the frequency of all the AC areas would have decreased, and all the generators would have output more power to balance the increased load. Therefore, it is reasonable to conclude that all sub-AC systems can share the primary frequency control function.
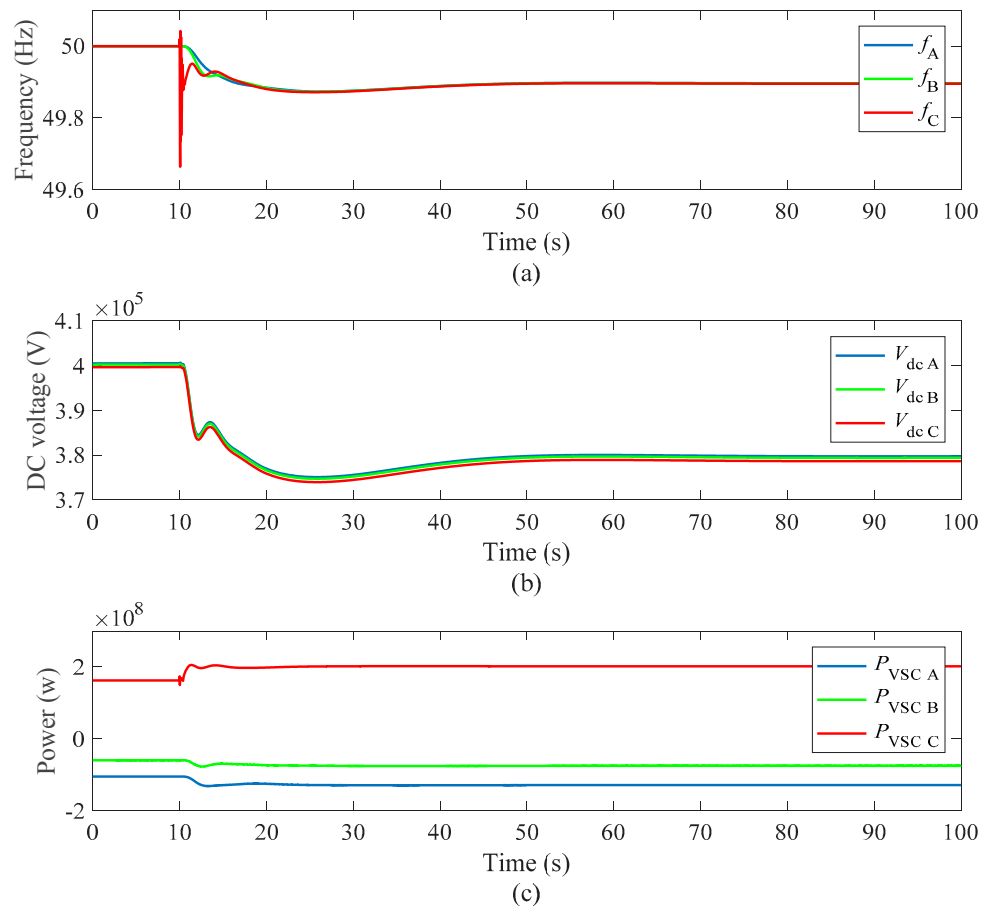

Figure 9. The waveforms of disturbances occurring in area C: (**a**) AC frequency of each sub-AC system, (**b**) DC-side voltage of each converter station, and (**c**) transmission power of each converter station.

The waveform of Figure 9 is similar to that in Figure 8, while the dynamic performance of Figure 9 is poor, as after 10 s, the frequency and DC voltage waveforms of Figure 9 have more fluctuation than the frequency and DC voltage waveforms of Figure 8. During load disturbance, the traditional control method will lead to more transient power fluctuations. This conclusion can also be found in reference [26]. Thus, it proves that the new control method is better than the traditional control method in terms of dynamic performance.

5.2. Secondary Frequency Control

Based on the simulation condition in Section 5.1, when the system became stable after load steps in area C, the active power of the generator in area B increased 45 MW at $t = 60$ s. This was just an imitation of secondary frequency control (considering that the generator in area B was the frequency control generator). The response waves of the frequency, the DC-side voltage, and the transmission power of each converter are shown in Figure 10. The response of the traditional control method is shown in Figure 11.
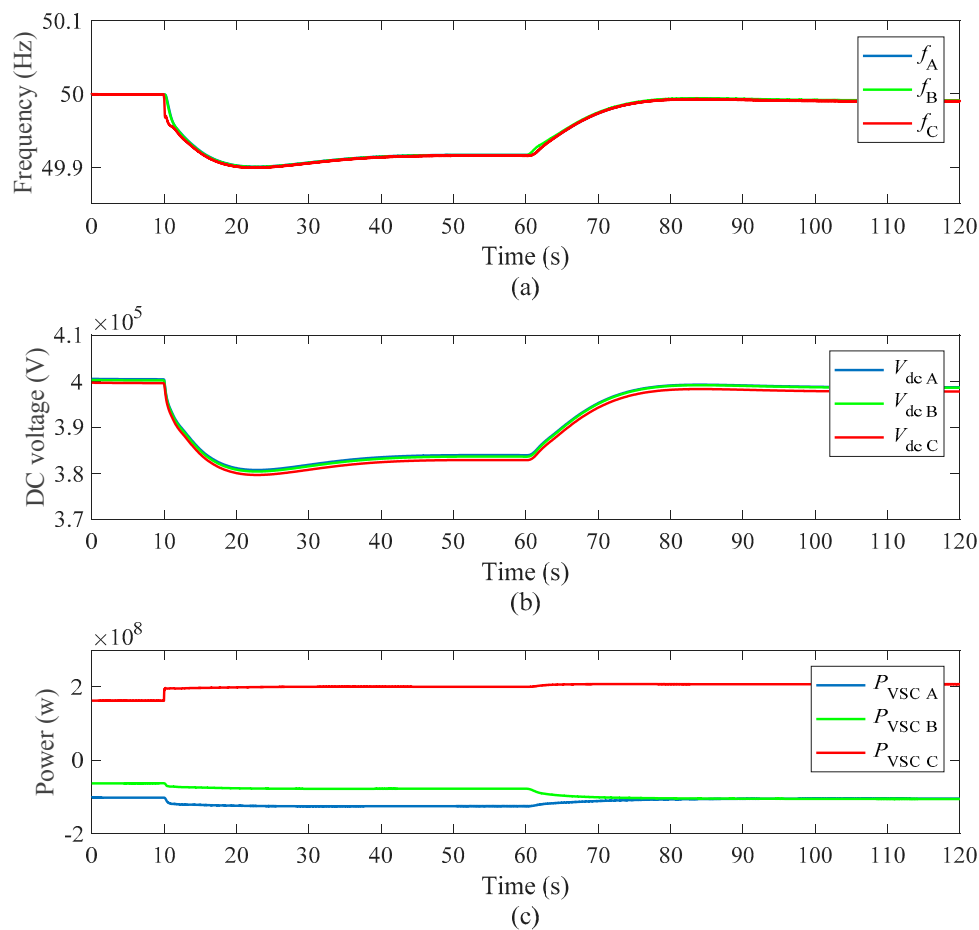
Figure 10. The waveforms of secondary frequency control: (**a**) AC frequency of each sub-AC system; (**b**) DC-side voltage of each converter station, and (**c**) transmission power of each converter station.

In Figure 9, both the AC frequency and DC voltage decreased after the load step occurred in area C at *t* = 10 s. The frequency waveforms of areas A, B and C were very similar. Thus, we could make an approximation, considering that the three frequencies were the same, to use their average value as the frequency of the hybrid AC/DC power system. In order to restore the AC frequency and DC voltage to the scheduled value, the secondary frequency control strategy could be introduced into the hybrid AC/DC power system. The average frequency was used to compute the output of the frequency control generator (e.g., the generator of area B). By increasing the active power output of the frequency control generator, the AC frequency and the DC voltage could be restored to the scheduled value. Therefore, when *t* = 60 s, the active power output of the generator in area B increased 45 WM (computed by using the decreased value of the average frequency).

As the frequency and DC voltage waveforms show in Figure 10, after the generator in area B increased 45 MW of active power at *t* = 60 s, the AC frequencies and DC voltages were restored to around the scheduled value. From the power waveform, the transmission power of station A was restored to the initial value. This means that the output of the generator in area A was restored to the initial value, while from the power waveform, the transmission power of station B increased (the waveform goes down, because it is a negative value). This means that the load step of area C was totally borne by the generator of area B. Thus, this demonstrates that, with the new converter control strategy, the AC/DC hybrid system could use the traditional secondary frequency control (the average frequency is considered as the frequency of the hybrid system). From this phenomenon, it is reasonable to suppose that when there is a power shortage in any AC area of the hybrid system, all the terminal DC voltages and all the AC area frequencies will decrease. In this situation, in order to

restore the AC frequencies and DC voltages to the scheduled value, the secondary frequency control strategy of traditional AC systems can be used. Because all the frequencies of different AC areas are very similar, and active power can be transferred automatically to meet the need (without a specified value), by increasing the suitable amount of active power output of the frequency control generator, the AC frequencies could be restored to the scheduled value. Thus, it is reasonable to conclude that, with the new control strategy of the converter station, it is easy to apply the secondary frequency control method of traditional AC systems to the AC/DC hybrid system.
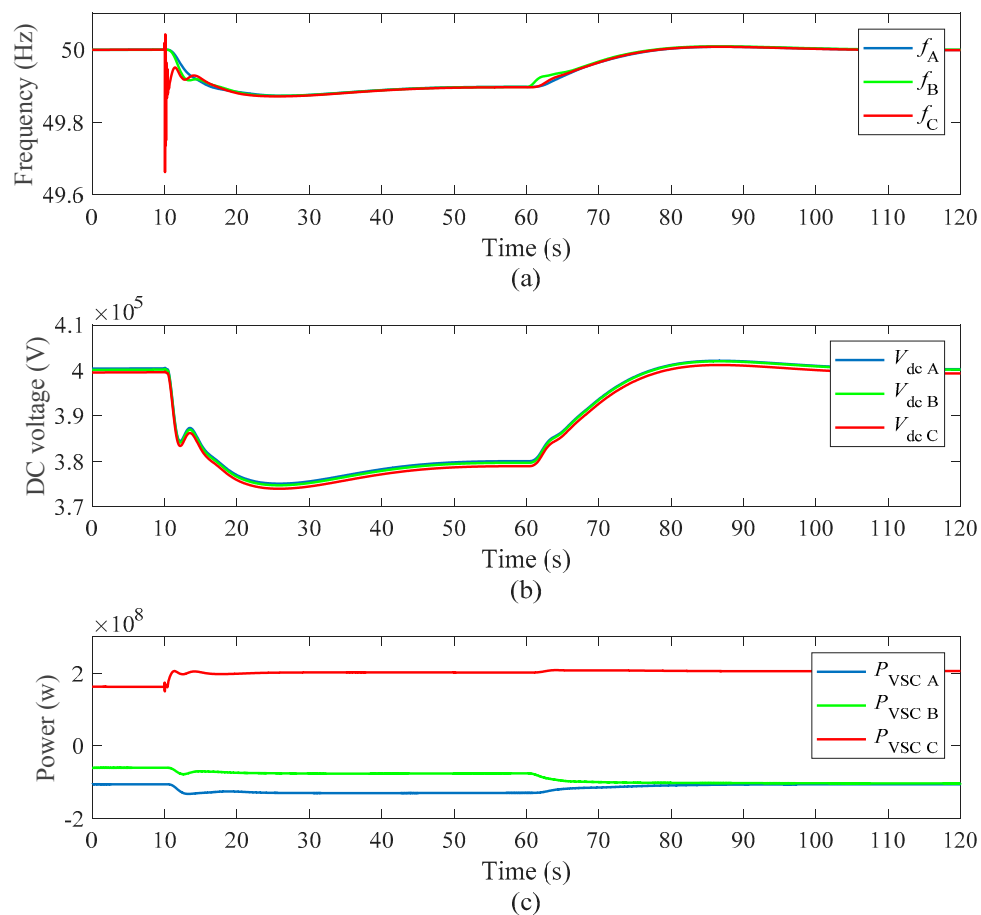

Figure 11. The waveforms of secondary frequency control: (**a**) AC frequency of each sub-AC system; (**b**) DC-side voltage of each converter station; and (**c**) transmission power of each converter station.

With the same simulation condition, the response of the traditional control method is shown in Figure 11. The waveforms of Figure 11 are similar to those of Figure 10, while the dynamic performance of Figure 11 is poor, as at $t = 10$ s and $t = 60$ s, the waveforms of Figure 11 have more fluctuation than for Figure 10. Thus, this proves that the new control method is better than the traditional control method in terms of dynamic performance.

6. Conclusions and Future Work

For the power balance control of multi-terminal VSC-HVDC systems, this paper improves the traditional converter station control mode by adopting the DC voltage and AC frequency slope (positive correlation) control mode. The paper adds a virtual moment of inertia into the control strategy. The control method has two functions. First, it supports different asynchronous AC systems sharing their primary frequency control function. Second, it is convenient for the AC/DC hybrid system to inherit the secondary frequency control methods of the traditional AC system. The simulation

results prove that the new control method is better than the traditional control method in terms of dynamic performance.

The new control method of the VSC-HVDC converter station has some potential value for further study. The frequency control strategy, grid-on and isolated island operation strategy and stability analysis will be researched in a follow-up study.

Author Contributions: Hao Wang and Yue Wang put forward to the main idea and designed the entire structure of this paper. Weihao Hu guided the simulation and paper writing. Guozhao Duan and Wenti Wang performed the simulation and analyzed the results critically. Zhe Chen made good suggestions in the article modification process and revised the paper.

Conflicts of Interest: The authors declare no conflicts of interest.

References

1. Adeuyi, O.D.; Cheah-Mane, M.; Liang, J.; Jenkins, N.; Wu, Y.; Li, C.; Wu, X. Frequency support from modular multilevel converter based multi-terminal HVDC schemes. In Proceedings of the 2015 IEEE Power & Energy Society General Meeting, Denver, CO, USA, 23 July–2 August 2015; pp. 1–5.
2. Andreasson, M.; Wiget, R.; Dimarogonas, D.V.; Johansson, K.H.; Andersson, G. Distributed primary frequency control through multi-terminal HVDC transmission systems. In Proceedings of the 2015 American Control Conference (ACC), Chicago, IL, USA, 1–3 July 2015; pp. 5029–5034.
3. Aouini, R.; Marinescu, B.; Kilani, K.B.; Elleuch, M. Improvement of transient stability in an AC/DC system with synchronverter based HVDC. In Proceedings of the 2015 12th International Multi-Conference on Systems, Signals & Devices (SSD), Sfax, Tunisia, 16–19 March 2015; pp. 1–6.
4. Babazadeh, D.; Freizadeh, F.; Nordström, L. Distributed ancillary service support for independent AC-areas through HVDC grid. In Proceedings of the 2015 IEEE PowerTech Eindhoven, Eindhoven, Netherlands, 29 June–2 July 2015; pp. 1–6.
5. Chaudhuri, N.R.; Chaudhuri, B. Adaptive Droop Control for Effective Power Sharing in Multi-Terminal DC (MTDC) Grids. *IEEE Trans. Power Syst.* **2013**, *28*, 21–29. [CrossRef]
6. Xu, L.; Yao, L.; Sasse, C. Power electronics options for large wind farm integration: VSC-based HVDC transmission. In Proceedings of the 2006 IEEE PES Power Systems Conference and Exposition, Atlanta, GA, USA, 29 October–1 November 2006; pp. 760–767.
7. Iov, F.; Sorensen, P.; Hansen, A.D.; Blaabjerg, F. Grid connection of active stall wind farms using a VSC based DC transmission system. In Proceedings of the 2005 European Conference on Power Electronics and Applications, Dresden, Germany, 11–14 September 2005; pp. 1–10.
8. Zhong, Q.C.; Weiss, G. Synchronverters: Inverters That Mimic Synchronous Generators. *IEEE Trans. Ind. Electron.* **2011**, *58*, 1259–1267. [CrossRef]
9. Li, Y.; Li, Y.W. Power management of inverter interfaced autonomous microgrid based on virtual frequency-voltage frame. *IEEE Trans. Smart Grid* **2011**, *2*, 30–40. [CrossRef]
10. Li, Z.P.; Song, W.X.; Zhong, Q.C. Virtual synchronous generator and its applications in micro-grid. *Proc. CSEE* **2014**, *34*, 2951–2963. (In Chinese)
11. Zhang, R.K.; Li, X.Y.; Yang, D.L. A frequency stability control strategy for interconnected VSC-MTDC transmission system. *Power Syst. Technol.* **2010**, *34*, 1–6. (In Chinese)
12. Wiget, R.; Andersson, G. Optimal power flow for combined AC and multi-terminal HVDC grids based on VSC converters. In Proceedings of the 2012 IEEE Power and Energy Society General Meeting, San Diego, CA, USA, 22–26 July 2012; pp. 1–8.
13. Mobarez, M.; Kashani, M.G.; Chavan, G.; Bhattacharya, S. A novel control approach for protection of multi-terminal VSC based HVDC transmission system against DC faults. In Proceedings of the 2015 IEEE Energy Conversion Congress and Exposition (ECCE), Montreal, QC, Canada, 20–24 September 2015; pp. 4208–4213.

14. Chen, H.R.; Zhang, F.; Chang, Y. Improvement of power quality by VSC based multi-terminal HVDC. In Proceedings of the 2006 IEEE Power Engineering Society General Meeting, Montreal, QC, Canada, 18–22 June 2006; pp. 1–6.

15. Chen, Y.; Dai, J.; Damm, G.; Lamnabhi-Lagarrigue, F. Nonlinear control design for a multi-terminal VSC-HVDC system. In Proceedings of the 2013 European Control Conference (ECC), Zurich, Switzerland, 17–19 July 2013; pp. 3536–3541.

16. Gonzalez-Longatt, F.M.; Roldan, J.M.; Rueda, J.L. Impact of DC control strategies on dynamic behaviour of multi-terminal voltage-source converter-based HVDC after sudden disconnection of a converter station. In Proceedings of the 2013 IEEE Grenoble PowerTech (POWERTECH), Grenoble, France, 16–20 June 2013; pp. 1–6.

17. Rouzbehi, K.; Zhu, J.; Zhang, W.; Gharehpetian, G.B.; Luna, A.; Rodriguez, P. Generalized voltage droop control with inertia mimicry capability-step towards automation of multi-terminal HVDC grids. In Proceedings of the 2015 International Conference on Renewable Energy Research and Applications (ICRERA), Palermo, Italy, 22–25 November 2015; pp. 1556–1561.

18. Fu, J.; Yuan, Z.; Wang, Y.; Xu, S.; Wei, W.; Luo, Y. Control strategy of system coordination in Nanao multi-terminal VSC-HVDC project for wind integration. In Proceedings of the 2014 IEEE PES General Meeting | Conference & Exposition, National Harbor, MD, USA, 27–31 July 2014; pp. 1–5.

19. Rao, H. Architecture of Nan'ao multi-terminal VSC-HVDC system and its multi-functional control. *CSEE J. Power Energy Syst.* **2015**, *1*, 9–18. [CrossRef]

20. Raza, A.; Dianguo, X.; Yuchao, L.; Xunwen, S.; Williams, B.W.; Cecati, C. Coordinated operation and control of VSC based multiterminal high voltage DC transmission systems. *IEEE Trans. Sustain. Energy* **2016**, *7*, 364–373. [CrossRef]

21. Chen, H.R.; Xu, Z. A novel DC voltage control strategy for VSC based multi-terminal HVDC system. *Autom. Electr. Power Syst.* **2006**, *30*, 28–33. (In Chinese)

22. Yao, L.Z.; Wu, J.; Wang, Z.B.; Li, Y.; Lu, Z.X. Pattern analysis of future HVDC grid development. *Proc. CSEE* **2014**, *34*, 6007–6020. (In Chinese)

23. Chaudhuri, N.R.; Majumder, R.; Chaudhuri, B. System frequency support through multi-terminal DC (MTDC) grids. *IEEE Trans. Power Syst.* **2013**, *28*, 347–356. [CrossRef]

24. Chen, Y.; Dai, J.; Damm, G.; Lamnabhi-Lagarrigue, F. A detailed study on a DC-voltage-based control scheme using a multi-terminal HVDC system for frequency control. In Proceedings of the 2013 European Control Conference (ECC), Zurich, Switzerland, 17–19 July 2013; pp. 3530–3535.

25. Haileselassie, T.M.; Uhlen, K. Primary frequency control of remote grids connected by multi-terminal HVDC. In Proceedings of the 2010 IEEE Power and Energy Society General Meeting, Minneapolis, MN, USA, 25–29 July 2010; pp. 1–6.

26. Paquette, A.D.; Reno, M.J.; Harley, R.G.; Divan, D.M. Sharing transient loads: Causes of unequal transient load sharing in islanded microgrid operation. *IEEE Ind. Appl. Mag.* **2014**, *20*, 23–34. [CrossRef]

27. Paquette, A.D.; Reno, M.J.; Harley, R.G.; Divan, D.M. Transient load sharing between inverters and synchronous generators in islanded microgrids. In Proceedings of the 2012 IEEE Energy Conversion Congress and Exposition (ECCE), Raleigh, NC, USA, 15–20 September 2012; pp. 2735–2742.

28. Machowski, J.; Bialek, J.; Bumby, J. *Power System Dynamics Stability and Control*, 2nd ed.; John Wiley & Sons, Ltd.: West Sussex, UK, 2008.